Ion Channels and Anisotropic Ion Mobility in a Liquid-Crystalline Columnar Phase As Observed by Multinuclear NMR Diffusometry

Anton E. Frise,[†,‡] Sergey V. Dvinskikh,[‡] Hiroyuki Ohno,[§] Takashi Kato,*[,†] and István Furó*[,‡]

Department of Chemistry and Biotechnology, School of Engineering, The University of Tokyo, Hongo, Bunkyo-ku, Tokyo 113-8656, Japan, Division of Physical Chemistry and Industrial NMR Centre, Department of Chemistry, Royal Institute of Technology, SE-10044 Stockholm, Sweden, and Department of Biotechnology, Tokyo University of Agriculture and Technology, Koganei, Tokyo 184-8588, Japan

Received: August 29, 2010; Revised Manuscript Received: October 13, 2010

The anisotropic diffusion of anions and cations in the columnar and isotropic phases of a fan-shaped imidazolium hexafluorophosphate salt is measured by ^{1}H and ^{19}F diffusion NMR experiments. The macroscopic orientation of the columnar phase is investigated by ^{2}H NMR spectroscopy. We find that the anions, confined by the cations, diffuse faster than the cations along the columns but slowly across them, which exemplifies the ion channel model of these materials. The cations and anions are dissociated in the columnar phase but are paired or clustered in the isotropic phase.

Introduction

Molecular self-organization has attracted a great deal of interest because it offers a promising avenue toward development of functional materials.[1−3] Self-assembled organic materials such as liquid crystals exhibit ordered, dynamic, and stimulus-responsive structures[4] which have proven potential in applications as soft materials with charge[5,6] and ion[7−14] transport and desirable optical properties.[15,16] As one example, ionic liquid-crystalline[7−14] molecules containing immiscible ionic and nonionic parts phase-separate on the molecular level and form various nanostructures in the bulk state. Those nanostructures can promote charge mobility by providing pathways for ion conduction on length scales many orders larger than the size of the involved molecules. Previously, we reported on the development of low-dimensional ion conduction in ionic liquid crystals.[7−12] In particular, one-dimensional ion conduction was achieved in self-assembled fan-shaped imidazolium salts exhibiting columnar phases that are stable in wide temperature ranges.[8−10,12] Uniaxial orientation of the columns could be obtained on a macroscopic scale by shearing thin samples, and the anisotropy of ion conductivity was observed by impedance measurements of such prealigned columnar samples. However, a more detailed characterization and understanding of the mobility of the ionic species in ionic liquid-crystalline materials are desirable to facilitate development of the dynamic properties of these materials.

In a recent study[13] on an ionic liquid exhibiting a bicontinuous cubic (Cub_{bi}) liquid-crystalline (LC) phase, we demonstrated that pulsed-field-gradient spin-echo NMR[17,18] is a powerful tool for studying the translational diffusion of different molecular and ionic species in ordered structures. In such diffusion NMR experiments, molecular selectivity can be achieved by observing nuclei with different gyromagnetic ratios (γ) to obtain the distinct diffusion coefficients of the different ionic species. Hence, we found[13] that cations and anions, dissociated in the liquid-crystalline phase and having exhibited different mobilities, form noncharged ion pairs or ion clusters in the isotropic phase. These results provide a molecular explanation to the ionic conductivity in the Cub_{bi} liquid-crystalline phase that is higher than that in the isotropic phase.[11]

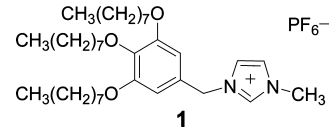

1

Figure 1. Fan-shaped imidazolium hexafluorophosphate salt **1** exhibiting a hexagonal columnar liquid-crystalline phase.

In addition to diffusion NMR, NMR spectroscopy of quadrupolar nuclei with spin quantum number $I > 1/2$ (e.g., ^{2}H with $I = 1$) provides an excellent tool for studying molecular orientation by observing the quadrupole splitting of spectral peaks. This is a well-established method to determine order parameters, phase transitions, and the extent of orientational disorder in liquid-crystalline materials[19] and has previously been successful in combination with diffusion anisotropy measurements not only in liquid crystals[20−25] but also in "soft" ion conductors.[26,27] One approach is to incorporate deuterons directly to the liquid-crystalline molecule. This is, however, a rather cumbersome method since it requires synthesis of deuterated samples. Another approach is to dissolve a minute amount of a small, anisotropic, and deuterated solute molecule in the liquid-crystalline phase and study its NMR signal.[28] A suitable probe should have a low volatility and a good solubility in the liquid-crystalline phase and must provide a strong enough signal also at low concentrations (<1 wt %) so that the self-assembled liquid-crystalline structure is not perturbed.

A fan-shaped imidazolium hexafluorophosphate salt (compound **1** depicted in Figure 1) has been shown to self-assemble in a liquid-crystalline hexagonal columnar phase extending from −33 to +78 °C on heating and from +73 to −38 °C on cooling.[10] The diameter of the columns was reported to be ca. 33 Å, and the anisotropy in the ion conduction has been

* To whom correspondence should be addressed. (T.K.) E-mail: kato@chiral.t.u-tokyo.ac.jp. Fax: (+81) 3-5841-8661. Phone: (+81) 3-5841-7440. (I.F.) E-mail: ifuro@physchem.kth.se. Fax: (+46) 8-790-8207. Phone: (+46) 8-790-8592.

† The University of Tokyo.

‡ Royal Institute of Technology.

§ Tokyo University of Agriculture and Technology.

10.1021/jp1082054
Published on Web 11/05/2010

observed.[10] Herein, we investigate the underlying mechanisms for this anisotropic behavior by the combined use of quadrupolar and diffusion NMR methods.

Experimental Section

Materials. The synthesis and thermal properties of compound **1** were previously reported.[10] Approximately 5 g of sample was prepared, and the purity was confirmed by solution NMR spectroscopy. Perdeuterated pyridine (d_5-pyridine) was obtained from Stohler Isotope Chemicals at 99.5% isotropic purity and used as received.

^{2}H NMR Spectroscopy. A small drop of d_5-pyridine (4 mg, 0.5×10^{-4} mol) was dissolved in a large amount of compound **1** (595 mg, 8.5×10^{-4} mol), directly into a 10 mm NMR tube. The sample was heated to the isotropic phase, where it was shaken vigorously to ensure complete mixing of the constituents. The low viscosity of the isotropic phase also allowed air bubbles to disappear from the sample. The boiling point of pyridine is approximately 115 °C, which is considerably higher than the melting point of compound **1** and the maximum temperature (91 °C) in this study; therefore, we do not expect significant evaporation of pyridine during our measurements.

^{2}H NMR measurements were performed on a Bruker DRX500 spectrometer (11.7 T) operating at 76.8 MHz for ^{2}H. The temperature at the sample position was calibrated with an external thermocouple with an accuracy of ca. 0.1 K. The sample was first cooled from the isotropic to the LC phase outside of the magnetic field, after which the sample was inserted into the magnet, where its ^{2}H NMR spectrum was obtained. Subsequently and having kept the sample in the magnetic field, the sample was heated to the isotropic phase, and several ^{2}H NMR spectra were obtained at different temperatures upon cooling (2 °C/min) from the isotropic to the LC phase.

Diffusion ^{1}H and ^{19}F NMR Spectroscopy. About 120 mg of compound **1** was added to a 5 mm NMR tube, and the sample was heated to the isotropic phase to remove air bubbles. The measurements were performed on a Bruker 500 Avance III spectrometer (11.7 T) operating at 500 MHz for proton (^{1}H) and 470 MHz for fluorine (^{19}F) and equipped with a Bruker microimaging probe (MIC5) and current amplifiers GREAT60. This probe has the capacity for generating magnetic field gradient pulses in three orthogonal directions with 2.8 T/m maximum gradient values. The gradient strengths in all directions were calibrated by measuring water diffusion (2.09×10^{-9} m^2/s for a 50 mol % H_2O-D_2O solution at 25 °C[29]). The temperature at the sample position was calibrated with an external thermocouple for both ^{1}H and ^{19}F probe inserts.

In the previously reported ionic conductivity measurements[10] the conductivities were obtained upon heating of prealigned samples. In our diffusion measurements the sample was therefore first cooled from the isotropic to the LC phase (to approximately 40 °C) inside the magnetic field. The diffusion measurement series were then performed upon a stepwise increase of the sample temperature from 40 °C. In the cation experiments, the ^{1}H signal from the methyl protons was exploited. The ^{19}F spectrum of the anion exhibited a doublet with a splitting of 715 Hz due to J coupling to ^{31}P. Longitudinal (T_1) and transverse (T_2) relaxation times were measured by conventional inversion−recovery and spin-echo experiments. At the lowest temperature reached in ^{1}H experiments these relaxation times were $T_1 = 0.9$ s and $T_2 = 1.5$ ms for the explored ^{1}H signal and $T_1 = 1.5$ s and $T_2 = 11.6$ ms for the ^{19}F signal. All relaxation times, in particular the transverse ones, increased with increasing temperature. The measured relaxation times were helpful when having set appropriate delay times in the diffusion NMR experiments where the stimulated-echo pulse sequence with an eddy-current delay was employed.[30] The diffusion time (Δ) was typically set to 500 ms and the gradient pulse length (δ) to 5 ms (for cation ^{1}H experiments) or 10 ms (for anion ^{19}F experiments). The gradient strength (G) was typically varied in 16 steps, with 16 scans acquired at each gradient strength step. The maximum gradient strength was chosen to provide signal decays by at least 1 and 2 orders of magnitude for ^{1}H and ^{19}F experiments, respectively. The gradient strength was limited to less than 90% of the maximum gradient for the probe (that is, <2.5 T/m). Other experimental parameters were typically set as follows: 90° pulse length to 6.5 μs, recycle delay to at least $5T_1$, eddy-current delay[30] to 30 ms, and gradient stabilization time to 1 ms. The obtained diffusional signal decays were used to calculate the diffusion coefficients.

Results

Quadrupolar NMR Spectroscopy. Prior to the diffusion measurements it was necessary to investigate whether the LC phase aligns in the magnetic field and the direction of that alignment. For this purpose we observed the spectral shapes of dissolved d_5-pyridine upon cooling the sample either inside or outside the magnet.

Figure 2a shows the temperature dependence of the ^{2}H NMR spectrum for the sample cooled inside the magnet from 91 to 54 °C, a temperature range which encompasses the isotropic−columnar phase transition temperature.[10] In the isotropic phase at high temperature, two peaks of relative intensity 3:2 are observed. The observation of two peaks is consistent with the known (ca. 1 ppm) isotropic chemical shift difference between deuterons at *ortho* and *para* + *meta* positions.[31] At 70 °C, the peaks split by approximately 1 kHz, which indicates that the sample transforms from an isotropic (disordered) to an anisotropic (ordered) phase. The size of the splitting increases slightly with decreasing temperature, indicating a small increase in order upon lowering the temperature. The phase transition temperature is essentially the same as that in the pure LC material (73 °C on cooling[10]), which verifies that the small amount of solute added has no influence on formation of the LC phase. The spectrum has an asymmetric shape which is plausibly caused by the overlap of the high-frequency satellites of the *ortho* and *para* + *meta* deuterons. The splitting on the low-frequency side is roughly 2 times the splitting in the isotropic spectrum. Hence, the spectral shape is consistent with a slightly different (by ca. 10%) quadrupolar splittings for the *ortho* and *para* + *meta* deuterons and by the different chemical shifts for them. (One should note that the chemical shift anisotropy whose static value is on the order of 5 ppm for aromatic hydrogens is scaled to a negligible value by the low−estimated to be on the order of 0.01 from the experimental quadrupole splitting−order parameter.)

A comparison of the ^{2}H NMR signals from the LC sample when cooled to 65 °C either outside or inside the magnet is shown in Figure 2b. The spectral shape for the former case is a broad powder pattern; i.e., the sample contains LC domains with their phase directors distributed randomly in three dimensions.[19] On the other hand, the spectrum obtained upon cooling inside the magnet consists of sharp peaks, which shows that the LC domains are aligned with respect to the magnetic field. The peak positions compared to the powder pattern indicate that the domains are aligned with their directors (here, the columnar axis) lying distributed in the plane perpendicular to the magnetic field;[28] i.e., we obtained an azimuthal distribution

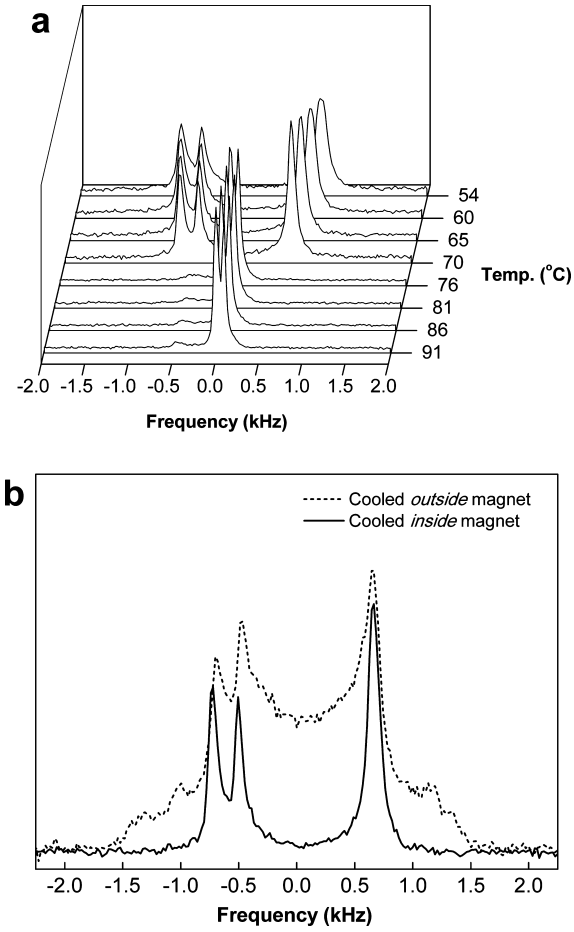

Figure 2. (a) ^{2}H NMR spectra of d_5-pyridine dissolved in compound **1** in a temperature range encompassing both isotropic and columnar liquid-crystalline phases. Quadrupole splitting of the d_5-pyridine peaks appears at the phase transition temperature (approximately at 70 °C upon cooling). (b) ^{2}H NMR spectra at 65 °C of d_5-pyridine dissolved in compound **1** in the LC phase. When the sample was cooled from the isotropic phase outside the magnet, an isotropic distribution of domain directors in three dimensions was obtained, as indicated by the typical powder pattern[19] of the spectrum. Cooling the sample from the isotropic phase inside the magnet leads to domain directors distributed in the plane perpendicular to the magnet field as shown by the coincidence of the oriented peak positions with the powder pattern peaks.

of the director. Analogous alignment of columnar phases in a magnetic field has been reported before.[21,32,33] The explanation for this alignment is the strong diamagnetic susceptibility of the aromatic benzene group in compound **1**, which favors orientation of compound **1** with the normal of the benzene plane perpendicular to the magnetic field direction.[28] When the molecules self-assemble upon cooling from the isotropic to the LC phase, intermolecular interactions of the oriented molecules favor the formation of LC domains with their directors perpendicular to the magnetic field. The size and mutual orientation (with the director in the confining plane) of adjacent domains may depend on other factors such as the sample purity or cooling speed.

Diffusion NMR Spectroscopy. To assess the anisotropy of diffusion for anions and cations in the material, we employed ^{19}F and ^{1}H NMR, respectively, to obtain signal decays by stimulated-echo experiments in a sample that had been pre-aligned in the magnetic field. Magnetic field gradients were applied in directions along the magnetic field (z direction) and perpendicular to the magnetic field (x/y direction). As was shown

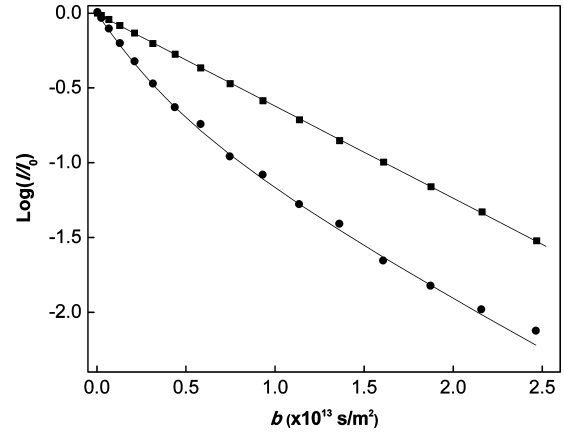

Figure 3. Decay of the ^{19}F signal from the hexafluorophosphate anion in stimulated-echo diffusion NMR experiments with the gradient direction parallel (z, ■) and perpendicular (x, ●) to the magnetic field at 65 °C and the best fits of the Stejskal−Tanner equation[34] and of eq 2 with two free diffusion coefficients to the data points (see also the text), respectively. b is the Stejskal−Tanner factor, $(\gamma G\delta)^2(\Delta - \delta/3)$.

by the ^{2}H NMR experiments in the aligned sample, columnar axes (coinciding with the phase director) lie in the x/y plane but are all perpendicular to the z direction. Hence, the diffusion coefficient obtained when applying a z gradient (D_z) corresponds to the diffusion of ions perpendicular to the phase director ($D_\perp$) and thus reports on molecular transport between columns. The obtained diffusional decays followed a straight line in a semilogarithmic plot (z gradient data in Figure 3); $D_\perp$ can therefore be obtained by fitting the z gradient decay data to the well-known Stejskal−Tanner equation,[34] with the Stejskal−Tanner parameter $b = (\gamma G\delta)^2(\Delta - \delta/3)$, where γ is the gyromagnetic ratio for the selected nucleus.

In contrast, when an x gradient (or a y gradient) is applied, the diffusional decay is influenced by diffusion both parallel ($D_\parallel$) and perpendicular ($D_\perp$) to the phase director. The outcome of this is dependent on the size of the LC domains. With small domains, molecules would sample all different diffusion directions during the time scale of the NMR diffusion experiment set by the diffusion time Δ; this would lead to a decay that is similar in character to the z gradient data in Figure 3 but providing instead the average diffusion coefficient:

$$D_{\mathrm{av}} = \frac{D_\parallel + D_\perp}{2} \tag{1}$$

For domains that are large as compared to the diffusional path length[18] of $(2D\Delta)^{1/2}$, each individual molecule exhibits a single diffusion coefficient, the size of which depends on the direction of the local director with respect to the direction of the applied gradient. Hence, the decay measured for the whole sample is a composite of decays with different decay constants, and the semilogarithmic plot will attain a curvature.[35] This is, indeed, the case for the x gradient data in Figure 3. However, domain sizes intermediate to the small and large limiting cases could also exhibit a decay which is curved in a semilogarithmic plot. Whether we have large, that is, $\gg(2D\Delta)^{1/2}$, domains can be decided by comparing diffusional decays obtained at different Δ values (see Figure 4). Since those signal decays virtually overlap, we can conclude we are not in the intermediate regime (where the curvature should vary by Δ), which means that at any $\Delta < 1000$ ms we are in the large domain limit; i.e., we are observing the diffusion anisotropy *within individual domains*.

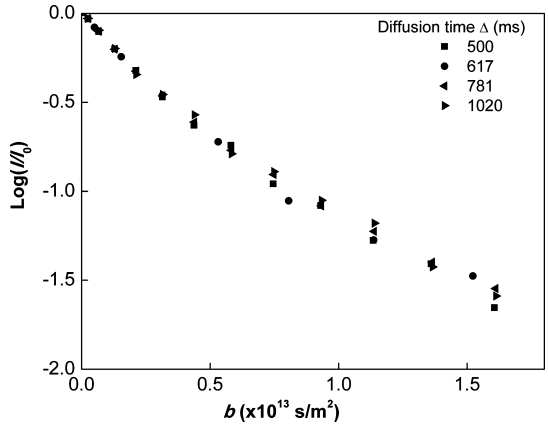

Figure 4. Effect of the diffusion time Δ on the decay of the ^{19}F signal from the hexafluorophosphate anion in stimulated-echo diffusion NMR experiments. b is the Stejskal−Tanner factor, $(\gamma G\delta)^2(\Delta - \delta/3)$. The direction of the applied magnetic field gradient, perpendicular (x) to the applied magnetic field (z), was within the plane over which the columnar director was distributed in the oriented liquid-crystalline sample. No significant variation of the decay with Δ indicates that the columnar domains are large relative to the diffusion path length.

To be on the safe side concerning this latter assessment and to achieve a good signal-to-noise ratio, we used $\Delta = 500$ ms in the following measurements (as also mentioned in the Experimental Section). For this diffusion time, the diffusional path length is calculated for the fastest diffusing element (anions in the liquid-crystal phase, D = ca. 10^{-12} m^2/s; see the results below) to be ca. 1 μm, which sets the lower bound of the domain size.

In the large domain regime, the observed decay is composed of decays with an azimuthal distribution of the two orthogonal diffusion coefficients $D_\perp$ and $D_{||}$. Assuming a random distribution of directors in the x/y plane,[35] the signal decay becomes

$$I/I_0 = \exp(-bD_\perp) \int_0^1 \exp\left(-b(D_{||} - D_\perp)x^2\right) \mathrm{d}x \qquad (2)$$

$D_\perp$ and $D_{||}$ can then be obtained from fitting with two free coefficients eq 2 to the experimental decays. As another alternative, one can exploit the results from the z gradient experiments, set $D_\perp = D_z$, and perform a single-free-coefficient fit of eq 2 to the decay data which then provides $D_{||}$.

To mutually verify the experimental accuracy of those methods, we shall present results from having them applied to the experimental ^{19}F diffusional decays with x gradients for PF_6^- anions in the LC phase. For the anions, both the signal-to-noise ratio and the diffusion anisotropy are high and the diffusional decays could be explored down to low signal intensities. Hence, the x gradient data in Figure 3 exhibit the decay data for PF_6^- at 65 °C with $\Delta = 500$ ms and the two-free-coefficient fit of eq 2 to that. The fit yields $D_\perp = (1.41 \pm 0.05) \times 10^{-13}$ m^2/s and $D_{||} = (7.29 \pm 0.15) \times 10^{-13}$ m^2/s. On the other hand, first obtaining $D_\perp = (1.37 \pm 0.05) \times 10^{-13}$ m^2/s from experiments with z gradients and then performing a single-free-component fit of eq 2 yielded $D_{||} = (7.22 \pm 0.15) \times 10^{-13}$ m^2/s. The quality of the fit as indicated by the coincidence of the fitted line with the experimental point is not distinguishable from that for x gradient data in Figure 3. The anisotropic diffusion coefficients obtained for the anion in a sample that has been magnetically aligned in the LC phase are presented in Figure 5 for all temperatures above 51 °C. Clearly, the two different evaluation methods yield consistent results.

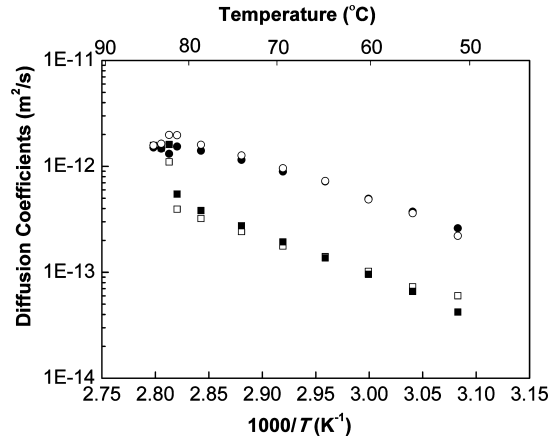

Figure 5. Diffusion coefficients for the hexafluorophosphate anion obtained by different methods (see also the text): two-free-coefficient fit to the data obtained by x gradients, yielding $D_{||}$ (○) and $D_\perp$ (□), and a single-free-coefficient fit, yielding $D_{||}$ (●) with $D_\perp$ (■), obtained from data recorded by z gradients (such as those seen in Figure 3). In the liquid-crystalline phase the anisotropy of diffusion ($D_{||}/D_\perp$) is roughly 5.

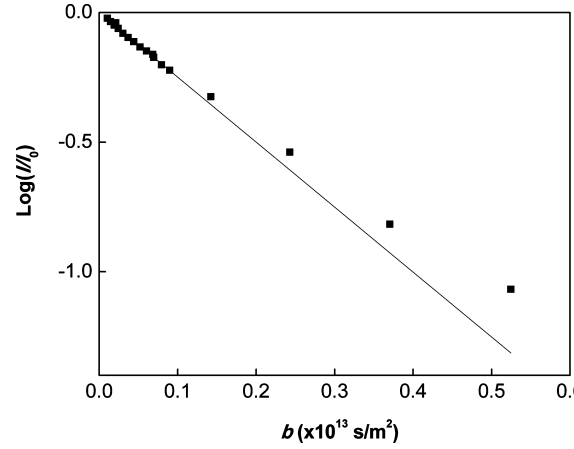

Figure 6. Decay of the ^{1}H signal from the imidazolium cation in a stimulated-echo diffusion NMR experiment with the gradient direction perpendicular (x) to the magnetic field (■) at 65 °C and best fit of the Stejskal−Tanner equation[34] to the initial part (ca. 20% signal reduction) of the decay. b is the Stejskal−Tanner factor, $(\gamma G\delta)^2(\Delta - \delta/3)$.

In the case of cations, the short (1.5 ms at the lowest explored temperature) transverse relaxation time T_2 led to a low signal-to-noise ratio in the stimulated-echo experiments, which did not allow recording of the diffusional decay to high attenuation. For the same reason, no cation diffusion measurements could be performed at temperatures lower than 62 °C. The limited decay (and the much smaller anisotropy of diffusion; see below) led to the cation signal decays recorded with x gradients showing only a very slight curvature (Figure 6). Hence, two-free-coefficient fits of eq 2 to the x gradient data led to results with low accuracy. The anisotropic diffusion coefficients of the cation, shown in Figure 7, were therefore obtained by the single-free-component fits, with $D_\perp$ obtained from experiments with z gradients.

Discussion

To facilitate the discussion, we replotted $D_{||}$ (Figure 8) and $D_\perp$ (Figure 9) for the two ionic species. Below, with the help of the features presented in Figures 5 and 7−9, we draw some conclusions concerning the structure and dynamics of the investigated phases.

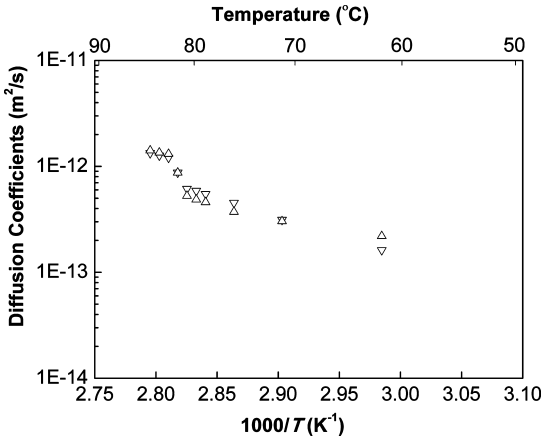

Figure 7. Diffusion coefficients for the cation, $D_{\|}$ (Δ) and $D_{\perp}$ (▽).

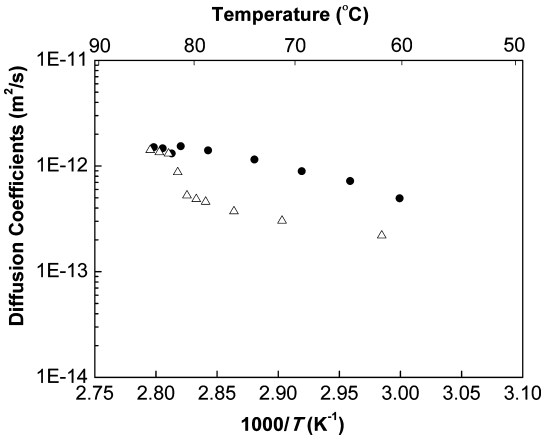

Figure 8. Diffusion coefficients along the columns ($D_{\|}$) for the hexafluorophosphate anion (●) and imidazolium cation (△). In the columnar phase, the anion diffusion is roughly 4 times faster than the cation diffusion.

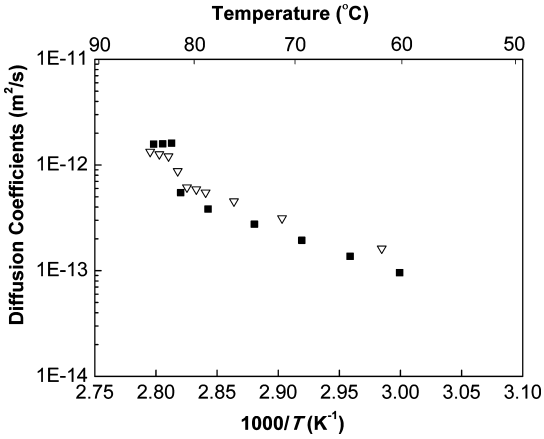

Figure 9. Diffusion coefficients perpendicular to the columns ($D_{\perp}$) for the hexafluorophosphate anion (■) and imidazolium cation (▽).

In the LC phase, the anion diffusion parallel to the phase director ($D_{\|}$), i.e., along columns, is approximately 5 times faster compared to the diffusion perpendicular to the phase director ($D_{\perp}$), i.e., across columns. At the columnar−isotropic transition, the difference between $D_{\|}$ and $D_{\perp}$ disappears (at 80 °C, close to the DSC-detected melting point of 78 °C, detected upon heating[10]). For the cation, there is negligible anisotropy, $D_{\|} \approx D_{\perp}$, and the columnar−isotropic transition is instead marked by a sudden increase of both diffusion coefficients. Remarkably,

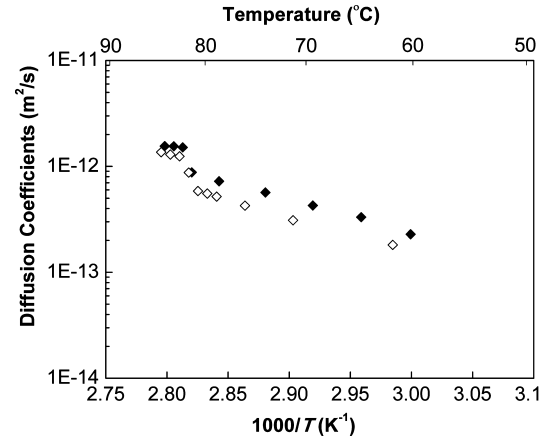

Figure 10. Isotropic average of the anisotropic diffusion for the hexafluorophosphate anion (◆) and the imidazolium cation (◇).

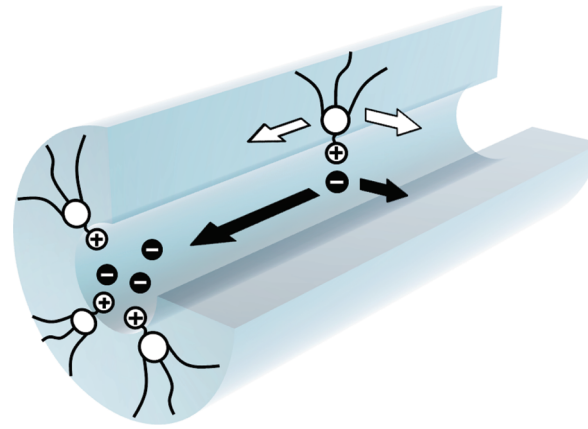

Figure 11. Illustration of the molecular structure and dynamics in and the ion-channel model of the investigated columnar phase.

the three-dimensional isotropic average of the anisotropic diffusion[20] (Figure 10)

$$D_{\mathrm{iso}} = \frac{2D_{\perp} + D_{\|}}{3} \tag{3}$$

behaves very similarly to the diffusion coefficient at the cubic−isotropic phase transition in another but similar system.[13] Namely, the small anions diffuse more than 50−60% faster in the LC phase than the large cations, but the diffusion coefficients of the two species become close (within approximately 20%) in the isotropic phase. This points to the same molecular scenario: dissociation in the columnar phase and significant pairing/clustering in the isotropic phase. Formation of uncharged ion pairs/clusters reduces the concentration of free ions and by that also the conductivity of the material. Another contribution to the increase of the cation diffusion coefficients $D_{\|}$ and $D_{\perp}$ upon the transition may come from a release of restriction on mobility caused by the ordered phase.

A comparison of the diffusion of anions and cations *along the columns* (Figure 8) shows that the anions diffuse ca. 4 times faster than the cations. In contrast, *perpendicular to the columns* (Figure 9) the anions move *slower* than the cations. These two observations provide a lucid illustration (and, indeed, a proof) of the ion channel model, depicted in Figure 11, of the nanostructure of this material in its columnar phase. The wall, made of cations with restricted molecular mobility, does what walls of a channel are supposed to do: it blocks the transverse

mobility of its content, the anions. Dissociated from the wall, the anions are restricted to the channels but can move rather freely along the channels.

Finally, the observed cation diffusion coefficients are much higher than that observed for molecules in a nonionic columnar phase.[21] The activation energy (obtained to be ca. 60 kJ/mol from the slope of the diffusion coefficients in the low-temperature part of Figure 7) is also lower, which indicates that this ionic columnar phase is, on the molecular level, more liquidlike than its nonionic counterpart.

Conclusions

We have in this study investigated the molecular mobility in a columnar ionic thermotropic liquid-crystalline material. In particular, we present NMR diffusion data obtained separately for the anionic and cationic molecular components. The diffusion is anisotropic and reveals that the columnar phase acts like a nanoscale conduction channel for the anions. The walls of the ion channel, made of the bulky cations, confine the small anions to the channel even though the molecular mobility within the wall is high. Within the channel, the anions are dissociated from the cations and can therefore move faster than the cations along the channel. These results provide a molecular-level explanation of the observed macroscopic conductivity features.

Acknowledgment. A.E.F. thanks the Swedish Foundation for International Cooperation in Research and Higher Education (STINT) and the Japan Ministry of Education, Culture, Sports, Science and Technology (MEXT) for scholarships. This work was partially supported by a Grant-in-Aid for Scientific Research (A) (No. 19205017; T.K.) from the Japan Society for the Promotion of Science (JSPS) and by the Swedish Research Council (VR).

References and Notes

(1) Tschierske, C. *J. Mater. Chem.* **2008**, *18*, 2869.
(2) Kato, T.; Mizoshita, N.; Kishimoto, K. *Angew. Chem., Int. Ed.* **2006**, *45*, 38.
(3) Kato, T. *Science* **2002**, *295*, 2414.
(4) Demus, D.; Goodby, J. W.; Gray, G. W.; Spiess, H.-W.; Vill, V. *Handbook of Liquid Crystals*; Wiley-VCH: Weinheim, Germany, 1998.
(5) Simpson, C. D.; Wu, J. S.; Watson, M. D.; Müllen, K. *J. Mater. Chem.* **2004**, *14*, 494.
(6) Yasuda, T.; Ooi, H.; Morita, J.; Akama, Y.; Minoura, K.; Funahashi, M.; Shimomuro, T.; Kato, T. *Adv. Funct. Mater.* **2009**, *19*, 411.
(7) Yoshio, M.; Mukai, T.; Kanie, K.; Yoshizawa, M.; Ohno, H.; Kato, T. *Adv. Mater.* **2002**, *14*, 351.
(8) Yoshio, M.; Mukai, T.; Ohno, H.; Kato, T. *J. Am. Chem. Soc.* **2004**, *126*, 994.
(9) Yoshio, M.; Kagata, T.; Hoshino, K.; Mukai, T.; Ohno, H.; Kato, T. *J. Am. Chem. Soc.* **2006**, *128*, 5570.
(10) Yoshio, M.; Ichikawa, T.; Shimura, H.; Kagata, T.; Hamasaki, A.; Mukai, T.; Ohno, H.; Kato, T. *Bull. Chem. Soc. Jpn.* **2007**, *80*, 1836.
(11) Ichikawa, T.; Yoshio, M.; Hamasaki, A.; Mukai, T.; Ohno, H.; Kato, T. *J. Am. Chem. Soc.* **2007**, *129*, 10662.
(12) Shimura, H.; Yoshio, M.; Hoshino, K.; Mukai, T.; Ohno, H.; Kato, T. *J. Am. Chem. Soc.* **2008**, *130*, 1759.
(13) Frise, A. E.; Ichikawa, T.; Yoshio, M.; Ohno, H.; Dvinskikh, S. V.; Kato, T.; Furó, I. *Chem. Commun.* **2010**, *46*, 728.
(14) Zhou, M. J.; Nemade, P. R.; Lu, X. Y.; Zeng, X. H.; Hatakeyama, E. S.; Noble, R. D.; Gin, D. L. *J. Am. Chem. Soc.* **2007**, *129*, 9574.
(15) Sagara, Y.; Kato, T. *Nat. Chem.* **2009**, *1*, 605.
(16) Iwata, T.; Suzuki, K.; Higuchi, H.; Kikuchi, H. *Liq. Cryst.* **2009**, *36*, 947.
(17) Callaghan, P. T. *Principles of Nuclear Magnetic Resonance Microscopy*; Clarendon Press: Oxford, U.K., 1991.
(18) Price, W. S. *NMR Studies of Translational Motion*; Cambridge University Press: Cambridge, U.K., 2009.
(19) Dong, R. Y. *Nuclear Magnetic Resonance of Liquid Crystals*; Springer: New York, 1994.
(20) Furó, I.; Dvinskikh, S. V. *Magn. Reson. Chem.* **2002**, *40*, S3.
(21) Dvinskikh, S. V.; Furó, I.; Zimmermann, H.; Maliniak, A. *Phys. Rev. E* **2002**, *65*, 050702.
(22) Wassall, S. R. *Biophys. J.* **1996**, *71*, 2724.
(23) Jóhannesson, H.; Furó, I.; Halle, B. *Phys. Rev. E* **1996**, *53*, 4904.
(24) Lindblom, G.; Orädd, G. *Prog. Nucl. Magn. Reson. Spectrosc.* **1994**, *26*, 483.
(25) Callaghan, P. T. *J. Chem. Phys.* **1983**, *79*, 6372.
(26) Li, J.; Wilmsmeyer, K. G.; Madsen, L. A. *Macromolecules* **2009**, *42*, 255.
(27) Hou, J.; Li, J.; Madsen, L. A. *Macromolecules* **2010**, *43*, 347.
(28) *NMR of Ordered Liquids*; Burnell, E. E., Lange, C. A. D., Eds.; Kluwer Academic Publishers: Dordrecht, The Netherlands, 2003.
(29) Mills, R. *J. Phys. Chem.* **1973**, *77*, 685.
(30) Gibbs, S. J.; Johnson, C. S. *J. Magn. Reson.* **1991**, *93*, 395.
(31) Pretsch, E.; Bühlmann, P.; Badertscher, M. *Structure Determination of Organic Compounds: Tables of Spectral Data*; Springer-Verlag: Berlin, 2009.
(32) *Nuclear Magnetic Resonance of Liquid Crystals*; Emsley, J. W., Ed.; Reidel: Dordrecht, The Netherlands, 1983.
(33) Sandström, D.; Nygren, M.; Zimmermann, H.; Maliniak, A. *J. Phys. Chem.* **1995**, *99*, 6661.
(34) Stejskal, E. O.; Tanner, J. E. *J. Chem. Phys.* **1965**, *42*, 288.
(35) Callaghan, P. T.; Söderman, O. *J. Phys. Chem.* **1983**, *87*, 1737.

JP1082054